Title:-

Longitudinal tracking reveals sustained polyclonal repopulation of human-HSPC in humanized mice despite vector integration bias

Gajendra W. Suryawanshi[1,2]; Hubert Arokium[1,2]; Sanggu Kim[6,7,8]; Wannisa Khamaikawin[4,5]; Samantha Lin[4]; Saki Shimizu[4]; Koollawat Chupradit[4]; YooJin Lee[1,2]; Yiming Xie[1,2]; Xin Guan[1,2]; Vasantika Suryawanshi[9]; Angela P. Presson[10,11]; Dong-Sung An[2,4]; Irvin S. Y. Chen[1,2,3#]

[1]Department of Microbiology, Immunology and Molecular Genetics, University of California, Los Angeles, Los Angeles, CA 90095, USA
[2]UCLA AIDS Institute, Los Angeles, CA, 90095, USA
[3]Division of Hematology-Oncology, David Geffen School of Medicine at UCLA, Los Angeles, CA 90095, USA
[4]School of Nursing, University of California, Los Angeles, CA, 90095, USA.
[5]Present address: Faculty of Medicine, King Mongkut's Institute of Technology Ladkrabang, Bangkok 10520, Thailand
[6]Department of Veterinary Biosciences, College of Veterinary Medicine, [7]Center for Retrovirus Research, [8]Infectious Disease Institute, The Ohio State University, Columbus, OH 43210, USA
[9]Department of Molecular and Computational Biology, University of Southern California, Los Angeles, CA, 90089, USA
[10]Division of Epidemiology, Department of Internal Medicine, University of Utah, Salt Lake City, 84108
[11]Department of Biostatistics, University of California, Los Angeles, 90095

#Corresponding authors:
Irvin S. Y. Chen;
615 Charles E. Young Dr. South
BSRB, Rm 173,
Los Angeles, CA 90095
syuchen@mednet.ucla.edu

Abstract:
Clonal repopulation of human hemopoietic stem and progenitor cells (HSPC) in humanized mouse models remains only partially understood due to the lack of a quantitative clonal tracking technique for low sample volumes. Here, we present a low-volume vector integration site sequencing (LoVIS-Seq) assay that requires a mere 25µl mouse blood for quantitative clonal tracking of HSPC. Using LoVIS-Seq, we longitudinally tracked 897 VIS clones—providing a first-ever demonstration of clonal dynamics of both therapeutic and control vector-modified human cell populations simultaneously repopulating in humanized mice. Polyclonal repopulation of human cells became stable at 19 weeks post-transplant indicating faster clonal repopulation than observed in humans. Multi-omics data of human fetal liver HSPC revealed that in vivo repopulating clones have significant vector integration bias for H3K36me3-enriched regions. Despite this bias the repopulation remains normal, underscoring the safety of gene therapy vectors. LoVIS-Seq provides an efficient tool for exploring gene therapy and stem cell biology in small-animal models.

Introduction:
Hemopoietic stem cells (HSC) are an ideal vehicle for introducing gene-modified cells to treat genetic disorders, cancers, and viral infections. Humanized mouse models—immunodeficient mice transplanted with human stem cells or tissues that generate a functioning human immune system—provide the most practical in vivo system for stem cell and disease research (reviewed in[1]). In particular, humanized bone marrow-liver-thymus mouse (hu-BLT mouse) models can support the development of T cells, B cells, monocytes, macrophages, and dendritic cells. Moreover, these hu-BLT mice demonstrate human MHC-restricted T cell response to Epstein-Barr virus (EBV) infection and human Dendritic cells-mediated T cell response against toxic shock syndrome toxin 1 (TSST1)[2]. Capable of mounting both innate and adaptive immune response, the hu-BLT mouse model is well-suited for antiviral gene therapy research. A recent study used an HIV-1 pre-infected hu-BLT mouse model to demonstrate that HIV-1 infection induces selective expansion of anti-HIV-1 dual shRNA gene-modified (protected) CD4+ T cells over control vector-modified unprotected CD4+ T cells[3]. However, whether the human HSPC in xenograft mouse models exhibit their human traits or clonally behave like mouse cells remains unclear.
Longitudinal clonal tracking in humans and macaques revealed biphasic expansion of transplanted HSPC: an early phase of rapid and transient expansion of short-term HSC and a late phase (~1 year post-transplant) of sustained expansion of long-term HSC[4,5]. However, clonal tracking in mice autologously transplanted with a limited number of barcoded HSC (marked with a unique sequence tag using lentiviral vector) showed that clones start to stabilize around week 12 post-transplant and progressively fewer clones contribute to the overall repopulation[6]. Another barcode tracking study in mice suggested transplantation dose-dependent

76 change in HSC differentiation[7]. However, generating a barcode library for every therapeutic test vector is
77 both cost-prohibitive and impractical; additionally, low DNA availability, lack of a universal barcode
78 counting method, and small barcode library size limit the accuracy of barcoding techniques. Finally, these
79 techniques lack the ability to identify genomic location of vector integration in host genomes.
80 In each transduced HSPC, the vector randomly integrates into the host genome, creating a unique vector-host
81 DNA junction sequence or VIS clone. A high-throughput integration sites (IS) sequencing assay can
82 simultaneously identify and track multiple VIS as well as detect probable mutagenic insertions. A
83 quantitative high-throughput VIS assay revealed that of all HSPC transplanted in rhesus macaques, ~0.01%
84 are long-term HSC and start contributing >1.5 years post-transplant[5]. Our long terminal repeat indexing–
85 mediated integration site sequencing (LTRi-seq) method enables multiplexed and unbiased quantitative
86 clonal analysis of cells gene-modified with anti-HIV or control vector and that of HIV-1 IS—all in the same
87 hu-BLT mouse[8]. VIS analysis at endpoint showed HIV-1 infection induced selective clonal expansion in the
88 anti-HIV (H1 LTR-index) gene-modified population without adverse impact on clonal expansion of the
89 control (H5 LTR-index) vector-modified population. However, only 100µl blood (0.6µg of DNA assuming
90 1000 cell/µl) can be drawn biweekly from a typical humanized mouse, which is insufficient for longitudinal
91 tracking with our VIS assay requiring ≥1µg DNA. Multiple displacement amplification (MDA), a whole
92 genome amplification technique, used to increase the DNA amount with a very low error rate (1 in 10^6 to 10^7
93 nucleotides)[9] and high coverage[10]. Due to low errors and high coverage, MDA can be used for various
94 sequence sensitive application such as single nucleotide polymorphism (SNP) and next generation
95 sequencing studies[11]. MDA-amplified DNA has been used to detect retroviral IS[12] and to sequence full-
96 length HIV-1 proviruses including the IS[13,14].
97
98 Although self-inactivating lentiviral vectors are low risk, a strong promoter within the vector can upregulate
99 the expression of endogenous genes where the vector integrated[15,16]. HIV-1 and HIV-1 based vectors are
100 known to favor transcriptionally active gene dense regions[17,18], with preference for histone modification H3
101 acetylation, H4 acetylation and H3K4 methylation[19]. Other studies found no preference for DNase I
102 hypersensitive sites[20] and H3K4 methylation being disfavored[21] and preference for H3K36me3 in Jurkat
103 cells[21]. The HIV-1 integration occurs with assistance from nuclear pore complex and targets the active genes
104 closer to the nuclear pore and disfavor heterochromatin regions and active regions located centrally in the
105 nuclease[22]. However, the implications of HIV-1 integration on cell fate are compounded by infection induced
106 cytotoxicity. An in vitro study using activated human CD34+ HSC also found lentiviral vector integration
107 preference for active genes[23]. These in vitro studies have tracked impact of vector integration on cell fate
108 over short time however long-term impact is only partially explored. Moreover, in human HSPC—more
109 specifically human fetal HSPC (FL-HSPC)— vector integration preference for epigenetic features is

110 unexplored. Importantly, influence of VIS-proximal epigenetic features on in vivo survival, proliferation,
111 and differentiation of gene-modified HSPC is unknown.
112 In this study, we present LoVIS-Seq, a combined MDA and VIS assay for low-volume samples. Using this
113 assay, we longitudinally track hundreds of clones in two different gene-modified cell populations
114 simultaneously repopulating in hu-BLT mice. This polyclonal repopulation resembles typical after-transplant
115 HSPC expansion in macaques and humans. In FL-HSPC, we found that vector integration in vivo detected
116 clones is biased for actively transcribed regions. Our method provides an efficient tool to study clonal
117 repopulation in murine and humanized-mouse models used for stem cell and gene therapy research.
118
119 **Results:**
120 *Minimum 10,000 bone marrow cells or 25µl blood is sufficient for LoVIS-Seq:*
121 To test our new assay, we collected bone marrow (BM) cells from hu-BLT (bone marrow-liver-thymus)
122 mouse (m860). Fetal liver CD34+ cells transduced with sh1005(anti-CCR5 shRNA)-EGFP vector or control
123 mCherry vector were mixed in equal ratio and transplanted in the mouse (Figure 1a-b, details in Methods).
124 We estimated clonal composition of the EGFP-WT (WT LTR-index) and mCherry-H1 (H1 LTR-index)
125 populations using unamplified bulk DNA, in triplicate, as described previously[8]. A total of 300 ±42 SD (216
126 ±22 SD mCherry-H1 VIS and 84 ±20 SD EGFP-WT) VIS were detected. The polyclonal profile in mouse
127 bone marrow (Figure 1c) resembled that found in hu-BLT mice[8] and in autologously transplanted mice[6],
128 nonhuman primates[5,24], and humans[4,25]. Next, to test our LoVIS-Seq assay (Figure 1d) that combines MDA
129 with VIS assays, we first performed MDA directly on 81,000, 27,000, 9,000, 3,000, and 1,000 bone marrow
130 cells, each in duplicate (Supplementary figure 1A, details in Methods section). Equal amounts of MDA-
131 amplified DNA and unamplified bulk DNA were used for the VIS assay (Supplementary table 1).
132 We found high reproducibility of clonal profiles in different MDA samples and within-MDA replicates of
133 81,000 to 9,000 cells (avg. Pearson's r value >0.91) (Figure 1e and Supplementary figure 1B-F); for less than
134 9,000 cells, the reproducibility dropped (avg. Pearson's r=0.87 for 3,000 and 0.73 for 1,000 cells).
135 Importantly, reduced cell numbers caused a modest reduction in VIS detection (Supplementary figure 1G).
136 These data validate that MDA-amplified DNA from >10,000 bone marrow cells is sufficient for LoVIS-Seq.
137 Next, to test accuracy of LoVIS-Seq with hu-BLT mouse blood, we collected 100µl blood at week 13, 15, 17
138 and ~1ml of whole blood at week 19 post-transplant. The hu-BLT mice were transplanted with an equal mix
139 of human CD34+ cells transduced with anti-HIV EGFP-WT vector and control mCherry-H5 vector (Figure
140 1f). Cells from 50µl blood were used for flow cytometry and the remaining cells were used for MDA
141 duplicates; each 25µl of blood (>10,000 human cells). High correlation (median Pearson's r =0.93) of
142 mCherry-H5 and EGFP-WT VIS clonal frequencies between unamplified and MDA-amplified DNA from
143 blood cells (Figure 1g) suggests that the clonal profile of entire mouse blood can be captured with 25µl of

144 blood. Importantly, the MDA replicates also showed high reproducibility (median Pearson's r>0.95,
145 Supplementary figure 3A). In conclusion, our LoVIS-Seq assay accurately captured the clonality of two
146 vector-modified cell populations in hu-BLT mouse blood using mere 25µl of blood or as few as 10,000 cells.
147 *LoVIS-Seq for simultaneous clonal tracking of therapeutic vector-modified and control vector-modified*
148 *populations:*
149 After demonstrating accuracy and reproducibility of MDA amplified DNA samples, we used 25µl of hu-
150 BLT mouse blood for LoVIS-Seq and LTR-indexes (Figure 1a, e) to track change in the relative frequencies
151 of 792 mCherry-H5 and 105 EGFP-WT VIS (897 total) clones over 6 weeks (Figure 2a). High correlations
152 between the total mCherry-H5 VIS clonal frequency and mCherry+ cell percentage by flow cytometry
153 (Pearson's r = 0.8) as well as between total EGFP-WT VIS clonal frequency and EGFP+ cells percentage
154 (Pearson's r = 0.9, Supplementary figure 3B) are consistent with our previous study[8]. Notably, the expansion
155 in EGFP-WT clones coincided with reduction of mCherry-H5 contribution and vice-versa (Figure 2b; solid
156 lines); these changes closely match the change in $EGFP^+$ and $mCherry^+$ cell percentages measured by flow
157 cytometry (Figure 2b; dashed lines). Furthermore, repopulation in both EGFP-WT and mCherry-H5
158 populations is largely driven by expansion of a few HSPC clones—a characteristic feature of after-transplant
159 repopulation. These results present a first-ever demonstration of clonal expansion of two populations,
160 therapeutic vector-modified and control vector-modified, simultaneously repopulating in hu-BLT mice.
161 Importantly, clonal data indicate two population competing to repopulate the mouse blood.
162 *Sustained polyclonal repopulation with rapid clonal expansion and stabilization:*
163 After identifying polyclonal repopulation of human cells in mice, we investigated the properties of its clonal
164 dynamics. The maximum number of VIS were detected at week 13 and on average, only 13% (±5%) fewer
165 VIS were detected at week 19 compared to week 13. Also, the number of total VIS contributing to
166 repopulation at each timepoint decreased with time (Figure 2c). On average, 61% (±12.8%) of persistent VIS
167 clones (m599: 235 clones, m598: 150 clones, and m591: 165 clones; total 550 clones) consistently
168 contributed for 6 weeks and provided stable polyclonal repopulation (Figure 2a area plots). While the
169 number of VIS clones steadily dropped over time in both the mCherry-H5 and EGFP-WT populations, their
170 clonal profiles became increasingly similar (Supplementary figure 4A-B), comparable to polyclonal
171 repopulation patterns that have been reported in nonhuman primates[5]. Moreover, correlation between time
172 points indicates clonal distribution at week 13 differs from week 19, with clonal expansion stabilizing around
173 week 17 (Supplementary figure 4B). We also examined Rényi's diversity[26] profiles for each animal at each
174 time point (details in Methods section). The clonal diversity at week 13 was highest and subsequently
175 decreased with time (Figure 2d). Diversities were similar between weeks 17 and 19 as indicated by their
176 overlapping diversity profiles. The Shannon[27] and Simpson[28] indices dropped between weeks 13 and 17,
177 indicating expansion of fewer clones (Supplementary figure 4C). The similarity of the indices between

178 weeks 17 and 19 suggests stabilization of clones. Contribution by the most frequent clone rose ~2.2 times,
179 from 0.078 (±0.005, n=3) at week 13 to 0.174 (±0.030, n=3) at week 17 (Figure 2e), signaling rapid
180 expansion of a few clones. Overall, the clonal repopulation remained normal despite faster expansion and
181 earlier stabilization of human HSPC clones in hu-BLT mice compared to humans, wherein stable clones
182 appear >1 year post-transplant[4].
183 *Clonal sharing between organs reveals normal repopulation and unique tissue distribution pattern:*
184 Our VIS data show normal clonal repopulation in blood of hu-BLT mice; however, in nonhuman primates,
185 the early post-transplant clonal expansion patterns differ between blood and organs[29]. We performed VIS
186 analysis on bulk cells from bone marrow (BM) and spleens of our hu-BLT mice to investigate whether the
187 tissue/organ clonal expansion pattern differed from blood. We found a very similar clonal expansion pattern
188 (avg. Pearson's r =0.94) between blood and spleen (Figure 3); however, clonal expansion in bone marrow
189 differed from blood and spleen. Interestingly, we observed that in all three tissue compartments, persistent
190 clones contributed the most to repopulation these results show normal clonal repopulation among the three
191 tissue compartments with substantial clonal sharing.
192 *Influence of genomic location and proximal genes on clonal growth:*
193 For each VIS, our assay provided both relative frequency and genomic location of integration allowing us to
194 monitor abnormal growth arising due to mutagenic insertions. Similar to the HIV-1 integration pattern[17], our
195 VIS data from in vivo repopulating clones showed preference for high gene density chromosomes
196 (Supplementary figure 5A). Additionally, similar genomic distribution of low, medium, and high frequency
197 in vivo repopulating VIS clones (Figure 4a) suggests clonal expansion is unrelated to genomic location of
198 integration. We found that in ~80% of the total detected clones, VIS occurred within ±1Kb of protein-coding
199 genes, significantly higher than 46% of 1000 random IS ($p < 0.001$, Supplementary figure 6A). About 8% of
200 VIS were within ±1Kb of long non-coding RNA (lncRNA) and 10% were outside ±1Kb of any genes (distal
201 VIS, Figure 4b inside pie chart). Persistent and top 10 VIS clones (top 10 most frequent VIS clones from
202 each timepoint) showed similar preference for gene biotypes (Figure 4B inside pie chart). Out of all VIS,
203 only 66 (including 1 out of 42 top 10 VIS) were proximal to known cancer consensus genes (Figure 4a
204 Circos plot). Gene ontology analysis of proximal genes and their mouse orthologs showed significant
205 enrichment ($P < 0.01$) in various biological pathways such as cell-cell interaction, viral process and
206 transcription regulation (Supplementary figure 5B). In vitro data for VIS-proximal gene in vector transduced
207 human CD34+ HSC showed enrichment in similar biological processes[23]suggesting that biological function
208 of VIS-proximal genes is unrelated to in vivo clonal expansion. Taken together, our results showed no clear
209 link between in vivo clonal expansion and genomic location of vector integration or biological function of
210 VIS-proximal genes.
211

212 *Integration bias for transcriptionally active genes in human fetal liver HSPC*:
213 Our data show VIS preference for genic regions, other studies using cell line and primary cells have reported
214 similar vector integration bias for active genes with low to moderate expression[18]. However, the
215 transcriptional state and expression level of the VIS-proximal genes is unknown in human FL-HSPC prior to
216 vector integration. To address this, we analyzed transcriptomic (RNA-seq) and functional genomic (ATAC-
217 seq and ChIP-seq) data from uncultured human FL-HSPC[30] isolated and processed using protocol identical
218 to one used in our study (see Methods). Owing to the direct biological relevance of human FL-HSPC to our
219 humanized BLT mice models, the multi-omics data is well suited to investigate the impact of vector
220 integration on stemness of vector-modified HSPC.
221 The gene expression (RNA-seq) data show that of all detected clones, including the persistent clones and top
222 10 VIS clones, >77% VIS are within ±1Kb of transcriptionally active genes (FPKM>1) (Figure 4b outer
223 donut chart). This is significantly higher than the ~27% of random IS proximal to active genes ($p < 0.001$,
224 Supplementary figure 6A). The level of transcriptional activity of VIS-proximal genes (based on the FPKM
225 value) was slightly higher than the median expression level of all active genes (Supplementary figure 5C).
226 Moreover, the median gene activity level (FPKM) varied based on gene biotype, with protein coding
227 proximal genes of all, persistent, and top 10 VIS clones having higher activity than lncRNA or pseudogenes
228 of proximal genes. Similar to in vitro observations[23] our in vivo clonal tracking data show VIS prefer active
229 genes but not highly active genes. These findings suggest that similar to in vitro, in vivo stability and
230 expansion of the HSPC clone is likely linked to expression level of VIS proximal gene.
231 *Vector integration favors actively transcribed regions:*
232 We speculate that the chromatin structure of active genes strongly influences vector integration. Previous in
233 vitro studies in cell lines suggested vector integration preference for genomic features such as select histone
234 modification and DNase I hypersensitivity sites using data from different cell lines. However, such analysis
235 is not available for human FL-HSPC and the effect of vector integration on stemness of these cells remains
236 unexplored. To investigate this, we analyzed functional genomic data for 10 different chromatin features in
237 uncultured FL-HSPC[30] (listed in Figure 5). These features include chromatin accessibility (ATAC-seq),
238 active RNA polymerase II, and 8 histone modifications (ChIP-seq). For VIS-proximal active genes
239 (FPKM>1), we found active transcription markers such as open chromatin region (ATAC-seq peaks) and
240 histone marks (e.g. H3K4me3) near TSS as well as H3K36me3 and H3K79me2-enriched regions within the
241 gene body. However, these marks were less prominent in inactive (FPKM<1) VIS-proximal genes (Figure 5a
242 profile plots and heatmaps). Random IS-proximal genes showed similar enrichment profiles in active genes
243 and their lack in inactive genes (Supplementary figure 6B). Further analysis found that out of 897
244 repopulating clones, 420 VIS (46% of total VIS) were within actively transcribed regions identified by
245 enrichment for histone-modification marks H3K36me3 and/or H3K79me2. This is significantly higher

246 compared to only 10% random IS within actively transcribed regions ($p<0.001$, Supplementary figure 6C).
247 Principal component analysis (PCA) on normalized enrichment levels (RPKM values) over a ±1Kb region of
248 VIS (Figure 5b data) clearly separated H3K36me3 and H3K79me2 from all other features and showed no
249 bias for random IS (Supplementary figure 7). Importantly, VIS avoided open DNA and transcription-
250 regulator histone marks H3K4me3 and RNApolII as well as repression marker H3K27me3 (Figure 5b and 5c
251 top panel). The top 10 most frequent VIS clones also displayed similar preference for all chromatin features
252 (Figure 5c middle panel) and comparatively, random IS were evenly distributed across all 10 histone marks
253 (Figure 5c bottom panel). Overall, the analysis reveals that vector integration in repopulating clones is a
254 significantly biased for H3K36me3 and/or H3K79me2 enriched regions. It should be noted that despite this
255 bias the clonal expansion of human HSPC in hu-BLT mice remained normal.
256
257 **Discussion:**
258 In this study we presented LoVIS-Seq, a new longitudinal clonal tracking method requiring a mere 25µl
259 blood or less to monitor clonal behavior of gene-modified cells in small-animal models. LoVIS-Seq
260 quantitatively captured the clonality of both control (mCherry-H1/H5) and anti-HIV (EGFP-WT)
261 populations in whole blood. We provide the first-ever demonstration of simultaneous polyclonal
262 repopulation of therapeutic vector-modified and control vector-modified cell populations in hu-BLT mouse
263 blood. The polyclonal expansion resembles normal post-transplant HSPC clonal repopulation in mice[6],
264 nonhuman primates[5,24] and humans[4,25]. Notably, the clonal frequency data recapitulated the flow cytometric
265 measurements. Persistent clones are major contributors in blood, BM, and spleen. The multi-omics data from
266 uncultured FL-HSPC revealed that vector integration in VIS clones that repopulated in mouse environment is
267 significantly biased toward H3K36me3 and/or H3K79me2 enriched regions. Remarkably, this vector
268 integration bias appears inconsequential with respect to clonal repopulation, as gene-modified HSPC
269 differentiated normally in vivo; this confirms the safety of our therapeutic and control lentiviral vectors.
270 We recently showed that in hu-BLT mice, monitoring clonal expansion of gene-modified and control
271 populations within the same animal gives an unbiased analysis[8] and allows a more direct assessment of
272 therapeutic vectors. In the current study, we longitudinally tracked both anti-HIV gene-modified and control
273 vector-modified populations in the same hu-BLT mouse. Interestingly, we found a competitive growth
274 pattern between two populations, with few clones from each population leading the expansion. The clonal
275 profiles in both populations resemble typical after transplant clonal repopulation confirming safety of both
276 vectors. Since safety and efficacy of multiple vectors can be tested in the same humanize mouse, LoVIS-Seq
277 can reduce both cost and time of vector development.
278 Previous studies propose that in myeloablated mice, hematopoiesis tends to stabilize around 22 weeks post-
279 transplant[7,31] while a recent study suggested 16 to 24 weeks[32]; our data indicates clonal stabilization between

280 17 to 19 weeks post-transplant. Overall, the clonal repopulation of human HSPC in hu-BLT mice resembles
281 that of mouse HSPC after autologous transplant. Cord blood HSPC transplanted in NGS mice also showed
282 similar clonal behavior, with clonal stabilization starting near week 18 to 20 post-transplant[33,34]. Although
283 the timescales compare well with other studies, caution is due considering high incidence of graft versus
284 host-disease-related illnesses in xenograft mouse models.
285 Analysis of repopulating VIS clones shows vector integration preference for transcriptionally active genes in
286 FL-HSPC however, RNA-Seq data indicates bias against highly expressed genes. For in vitro activated cord
287 blood and BM derived CD34+ HSC, the lentiviral vector showed no preference for highly active genes[23].
288 This is likely due to either obstruction by transcriptional machinery or detrimental effect of vector integration
289 on survival of the cell. Investigation of 10 chromatin features showed strong VIS bias toward actively
290 transcribed regions marked by histone modifications H3K36me3 and H3K79me2. This bias could be
291 attributed to LEDGF/p75, a chromatin binding protein essential for efficient HIV-1 integration[35,36], that binds
292 to integrases of HIV-1[37,38] and protects the pre-integration complex from degradation[39], whereas the N-
293 terminal PWWP domain of LEDGF is known to preferentially interact with H3K36me3[40,41]. H3K79me2 and
294 H3K36me3 mark the gene body[42] and H3K36me3 marks exons and is positioned near the 5` end of the exon
295 and is correlated with alternative splicing[43,44]. Thus, VIS in proximity of H3K36me3 are likely to influence
296 co-transcriptional splicing of the proximal gene as well as expression of the vector itself. In vivo
297 repopulating clones having significant vector integration bias for H3K36me3 may be linked to survival of
298 clones in vivo requiring further investigation. However, tracking of hundreds of single HSPC clones suggests
299 that such transcription events have miniscule to no impact on the stemness of repopulating vector-modified
300 HSPC.
301 A recent study demonstrated use of CRISPR/Cas to introduce barcodes in the long-term HSPC and
302 longitudinally tracked a very limited number of HSPC clones[34]. Comparatively, using LoVIS-Seq we have
303 tracked ~10 times more HSPC clones per animal with high accuracy and reproducibility. It is pertinent to
304 note that to enable insertion of barcoded donor DNA into the host genome, HSPC need to undergo in vitro
305 preconditioning and incubation before transplantation. The double stranded breaks introduced by
306 CRISPR/Cas activate DNA damage responses causing significant delays in HSPC proliferation and affects
307 their in vivo repopulation[45]. Additionally, off-target gene-editing by CRISPR/Cas remains a concern. In
308 contrast, LoVIS-Seq does not require preconditioning of HSPC and provides a ready to use high-throughput
309 clonal tracking assay for small-animal models. Furthermore, LoVIS-Seq has wider applicability owing to its
310 adaptability to many lentiviral vectors commonly used to insert transgenes or reporter gene such as GFP.
311 LoVIS-Seq with whole genome amplification allows for quantitative assessment of clonal behavior in small-
312 animal models. However, the accuracy and reproducibility of our assay depends on the initial number of
313 cells used for MDA (Figure 1d). To minimize sampling errors, it is important to have a sufficient number of

314 gene-marked human cells in each 25µl of blood or 10,000 cells to represent each clone in similar proportions
315 as in the bulk population. Higher human reconstitution and gene marking are often desirable and necessary
316 conditions wherein our assay provides optimal results.
317 Overall, using a mere 25µl blood and LTR-indexed vectors, we explored polyclonal expansion in both
318 control and therapeutic vector-modified populations in the same hu-BLT mice. LoVIS-Seq revealed the in
319 vivo dynamics of clonal expansion, emergence of stable stem cell clones, and consequences of vector
320 integration bias on repopulation. Thus, LoVIS-Seq provides an efficient tool for multifaceted analysis of
321 clonal dynamics in murine and humanized-mouse models that are used extensively in HIV, cancer, gene-
322 therapy, and stem cell research.
323
324 **Methods:**
325 *Human fetal thymus and isolation of FL-CD34+ cells from fetal tissue*
326 Human fetal thymus and livers were obtained from Advanced Bioscience Resources (ABR) and the UCLA
327 CFAR Gene and Cellular Therapy Core. Human fetal liver CD34+ HSPC and thymus pieces were processed
328 as previously described[46]. Briefly, a single cell suspension of fetal liver cells was strained through 70 µm
329 mesh and layered onto density gradient separation media (Ficol Paque PLUS, GE Healthcare). After 20
330 minutes of centrifugation, the mononuclear cells layer was collected. Anti-CD34+ microbeads (Miltenyi
331 Biotech) were used for magnetic isolation of CD34+ cells from mononuclear cells. Calvanese et al.[30] also
332 obtained fetal liver from the UCLA CFAR Gene and Cellular Therapy Core and followed identical CD34+
333 magnetic sorting to isolate uncultured FL-HSPC for RNA-seq, ATAC-seq, and ChIP-seq assay.
334 *Humanized BLT mouse and sample collection*
335 NOD.Cg-*Prkdc*^{scid}*Il2rg*^{tm1Wjl}/SzJ (NSG) mice, 6-8-week-old, were myeloablated 1 day before transplant by
336 intraperitoneal (i.p.) injection with 10 mg/kg of 6-thioguanine (6TG) (Sigma-Aldrich, Saint Louis, MO) or
337 35mg/kg of Busulfan for mouse m860. Myelo-preconditioned mice were transplanted with human fetal liver
338 CD34+ HSPCs transduced with Anti-HIV vector (EGFP+) (0.5×10^6 cells/mouse) and mixed with HSPCs
339 transduced with the control (mCherry+) vector (0.5×10^6 cells/mouse). The mice were transplanted with a
340 two-step procedure: half the mixture of EGFP+ and mCherry+ transduced cells was solidified by matrigel
341 (BD Bioscience, San Jose, CA), mixed with CD34- cells as feeder cells (4.5×10^6 cells), and implanted with a
342 piece of human thymus under the mouse kidney capsule. Then, mice were injected with the other half of the
343 mixed EGFP+ and mCherry+ transduced cells via retro-orbital vein plexus using a 27-gauge needle on the
344 same day. Bone marrow cells for MDA were harvested from mouse m860 at week 25 post-transplant. For
345 longitudinal clonal tracking and to monitor human leukocyte reconstitution and percentage of the EGFP+
346 and mCherry+ marked cells, 100µl of mouse blood was collected from the retro-orbital vein every two
347 weeks from weeks 13-19 post-transplant. Plasma was removed and peripheral blood cells were stained with

348 monoclonal antibodies for 30 minutes. Red blood cells were lysed with red blood cell lysis buffer (4.15 g of
349 NH4Cl, 0.5 g of KHCO3, and 0.019 g of ethylenediaminetetraacetic acid in 500 mL of H2O) for 10 minutes
350 and washed with FACS buffer (2% fetal calf serum in phosphate-buffered saline [PBS]). Stained cells were
351 resuspended in 16µl PBS, of which 8µl was split equally into two tubes for MDA replicates. The remaining
352 8µl was mixed with 300µl of 1% formaldehyde in PBS and examined with Fortessa (BD Biosciences) flow
353 cytometers. Flow cytometry data was utilized to monitor human reconstitution (Supplementary table 2) and
354 count human cells, mCherry+ cells, and EGFP+ cells as well as human T and B cells in blood
355 (Supplementary figure 2). The following monoclonal antibodies with fluorochromes were used: human
356 CD45-eFluor 450 (HI30, eBioscience), CD3-APC-H7 (SK7: BD Pharmingen), and CD19-BV605 (HIB19:
357 BioLegend). Data were analyzed on FlowJo (TreeStar, Ashland, OR) software.
358 The UCLA Institutional Review Board has determined that fetal tissues from diseased fetuses obtained
359 without patient identification information are not human subjects. Written informed consent was obtained
360 from patients for use of these tissues for research purposes. All mice were maintained at the UCLA Center
361 for AIDS Research (CFAR) Humanized Mouse Core Laboratory in accordance with a protocol approved by
362 the UCLA Animal Research Committee.
363
364 *LoVIS-Seq workflow with whole genome amplification and quantitative VIS assay*
365 Multiple displacement amplification for whole genome amplification: To estimate the minimum number of
366 cells required for LoVIS-Seq, we collected 81,000, 27,000, 18,000, 9,000, 3,000, and 1,000 bone marrow
367 cells from mouse m860 by serial dilution and stored in 4µl of PBS at -20ºC. MDA was done directly on cells
368 using the REPLI-g Single Cell Kit from Qiagen (Cat #150343) following kit-specific protocol. For
369 longitudinal clonal tracking in the blood compartment, 100 µl blood was drawn at weeks 13, 15 & 17. At end
370 point (week 19), max blood (≈ 1ml) was collected, out of which 100µl was used for flow cytometric analysis
371 along with MDA; the remainder was used to isolate unamplified whole blood DNA. Cells for MDA were
372 isolated as described above and stored in 4µl of PBS at -20ºC. MDA-amplified DNA was then used for
373 quantitative VIS assay. A Qiagen DNeasy Blood & Tissue Kit was used to extract unamplified DNA from
374 max blood cells, splenocytes, and bone marrow cells.
375
376 Quantitative VIS assay and data analysis workflow: For VIS sequencing, we followed the procedures
377 described in our previous publication[5,8,47,48] and focused on analyzing only the right LTR junctions using
378 CviQI and RsaI restriction enzymes. For our VIS assay we used one microgram MDA-amplified or
379 unamplified genomic DNA for animal m860 samples and two micrograms MDA-amplified or unamplified
380 genomic DNA for different time point samples, with a few exceptions (see Supplementary Tables 1 and 2).
381 DNA samples were subject to extension PCR using LTR specific biotinylated primers

382 /5BiotinTEG/CTGGCTAACTAGGGAACCCACT 3' and /5BiotinTEG/CAGATCTGAGCCTGGGAGCTC
383 3'. The extension PCR product was then digested using CviQI and RsaI restriction enzymes and biotin
384 primer bound DNAs isolated using streptavidin-agarose Dynabeads using magnetic separator as per
385 manufactures instructions. The vector-host junctions capture on streptavidin beads were processed for linker-
386 mediated PCR (LM-PCR) methods as described previously[47,48]. The linker ligated vector-host junction DNA
387 was subjected to two step PCR. First step amplification was done using primer 5'
388 CTGGCTAACTAGGGAACCCACT 3' and first linker primer GTGTCACACCTGGAGATAT. We
389 removed the internal vector sequence by restriction enzyme (SfoI) digestion. The digested product of first
390 PCR was then amplified using primer 5'ACTCTGGTAACTAGAGATCC 3' and second linker primer 5'
391 GGAGATATGATGCGGGATC 3'. Since the LTR index sequence is included in the vector-host junction
392 the we obtain unbiased amplification all the H1, H5 and/or WT VIS sequences. Lentiviral vectors used in
393 this study as derived from FG12-mCherry lentiviral vector[46] and all the primers are designed accordingly. A
394 detailed protocol for VIS assay is provided in supplementary text. The amplicon libraries prepared using
395 custom made Illumina sequencing primers for Illumina MiSeq (m860 samples) or iSeq100 (m599, m599,
396 and m591 samples) sequencer. Sequences with a virus-host junction with the 3' end LTR, including both the
397 3'-end U5 LTR DNA and ≥ 25 base host DNA (with ≥ 95% homology to the human genome), were
398 considered true VIS read-outs. The sequence mapping and counting method was performed as described
399 previously[8]. In brief, sequences that matched the 3'end LTR sequence joined to genomic DNA as well as
400 LTR-indexes (H1, H5 or WT) were identified using a modified version of SSW library in C++[49]. Reads
401 were classified as H1, H5, or WT VIS based on the LTR barcodes used in the experiment. VIS sequences
402 were mapped onto the human genome (Version hg38 downloaded from https://genome.ucsc.edu/) using
403 Burrows-Wheeler Aligner (BWA) software. Mapped genomic regions were then used as reference and VIS
404 reads were remapped using BLAST to further remove poorly mapped reads to get an accurate estimate of
405 sequence count. Final VIS counting was done after correcting for VIS collision events and signal crossover
406 as described previously. VIS with a final sequence count less than the total number of samples analyzed per
407 animal were removed. VIS clones with maximum frequency values below 1st quartile were classified as "low
408 frequency", clones with maximum frequency value above 3rd quartile were classified as "high frequency",
409 and clones with maximum frequency between the 1st and 3rd quartiles were designated "medium frequency".
410 VIS clones that were detected with frequency >0 at every week from 13-19 are termed "persistent clones".
411 The 10 high frequency VIS clones at each timepoint were selected as top 10 VIS. All the VIS data and list of
412 VIS-proximal genes is provided in supplementary file.
413 *Random integration sites*

414 Random integration sites were generated in silico using a custom python script. To mimic our VIS assay, we
415 randomly selected 1000 integration sites that were within ±1500bp of the nearest CviQI/RsaI (GTAC) site in
416 the human genome (hg38).

417 *Clonal diversity analysis*

418 For diversity analysis, we used Rényi's diversity/entropy[26] of order α defined as follows

419 $$H_\alpha = \frac{1}{1-\alpha}\log\left(\sum p_i^\alpha\right),$$

420 where p_i is the proportional abundance of the ith VIS clone for $i = 1, \ldots, n$. At each timepoint, an average
421 Rényi's diversity profile was obtained by calculating average values of $\boldsymbol{H_\alpha}$ for $\alpha \geq 0$. The α is considered as
422 a weighting parameter such that increasing α leads to increased influence of high frequency VIS clones. The
423 proportional abundance is calculated as $p_i = s_i/S$, where s_i is the sequence count of the ith VIS clone and S
424 is the sum of sequence counts from all VIS clones. The Rényi's diversity $\boldsymbol{H_\alpha}$ values are averaged over two
425 replicates and plotted as a function of α. If all VIS clones contributed equally, i.e. $p_i = \frac{1}{n}$ for all $i = 1, \ldots, n$,
426 then $\boldsymbol{H_\alpha}$ for all values of α would be equal and the profile (line) would be horizontal. VIS clones expanding
427 at different rates would show decreasing $\boldsymbol{H_\alpha}$ values as α increases, generating a downward-sloped diversity
428 profile that is steeper with more non-uniform clonal expansion. $\boldsymbol{H_\alpha}$ indicates clonal diversity of the
429 repopulating cells, such that consistently higher values of $\boldsymbol{H_\alpha}$ indicate a more diverse clonal population. If
430 the profiles for two populations/samples cross, then their relative diversities are similar. For $\alpha = 0$, $\boldsymbol{H_0} =$
431 $\log(n)$ and the antilogarithm of this value equates to the richness or number of unique IS. $\boldsymbol{H_\alpha}$ at $\alpha = 1$ and
432 $\alpha = 2$ are the Shannon and 1/Simpson indexes, respectively. We calculated Renyi's diversity using the R
433 package BiodiversityR (*https://cran.r-project.org/web/packages/BiodiversityR/index.html*). For the above
434 analysis, we used raw sequence counts from two replicates without distinguishing between mCherry-H5 VIS
435 and EGFP-WT VIS.

436 *RNA-seq data analysis*

437 Raw sequence data of uncultured FL-HSPC (in triplicate) was pre-processed for quality using Fastqc.
438 Trimmomatic was used to remove adaptors and for quality trimming. After this, reads were aligned onto
439 human genome hg38 using RNA STAR aligner[50]. SAMtools was used to remove reads with low mapping
440 scores (< 20) and to generate BAM files. Cufflinks[51] was used to calculate FPKM values for all genes. The
441 human cancer consensus gene list is from Catalogue of Somatic Mutations In Cancer
442 (https://cancer.sanger.ac.uk/census).

443 *ATAC-seq analysis*

444 Raw sequence data of uncultured FL-HSPC (in triplicate) was pre-processed for quality using Fastqc.
445 Adaptor removal and quality trimming was done using Trimmomatic. After this, reads were mapped onto
446 human genome hg38 using bowtie2 with parameter --very-sensitive -X 2000 -k 1. SAMtools was used to

447 remove reads with low mapping (<20) scores, blacklisted regions[52], and to generate BAM files. Picard tool
448 kit was used to remove duplicate reads. We used Genrich, a paired end peak caller, to identify ATAC peaks.
449 Software deepTools[53] was used to generate coverage (.bw) files and for visualization of open DNA in genes
450 and VIS-proximal regions.
451 *ChIP-seq data analysis*
452 Raw sequence data of uncultured FL-HSPC for histones, RNAploII, and input were pre-processed for quality
453 using Fastqc. Trimmomatic was used to remove adaptors and for quality trimming. After this, reads were
454 mapped onto human genome hg38 using bowtie2 with parameter --local. SAMtools was used to remove
455 reads with low mapping (<20) scores, blacklisted regions[52], and to convert SAM to BAM format. Picard tool
456 kit was used to remove duplicates. MACS2 tool was used to call peaks for all histone marks and RNApolII
457 using input sample as control. Software deepTools[53] was used to generate coverage .bw files and for
458 visualization of histone/RNApolII in genes and VIS proximal regions.
459 *Statistical analysis*
460 Clonal frequencies are summarized as means ± standard deviations (SDs). Pearson correlations are used to
461 compare the similarity and reproducibility of clonal profiles between two samples and replicates,
462 respectively. Pearson's r values and p values are calculated using statistical software R (version 3.6,
463 https://www.r-project.org/). To determine if VIS preference for genomic and epigenetic features differs
464 significantly from random IS, we used Pearson's chi-squared test with Yate's continuity correction (function
465 chisq.test() in software R). We use Principle component analysis (PCA) to reduce the complexity of read
466 coverage data of multiple chromatin feature in proximity to VIS. The dimensionality reduction by PCA
467 method is similar to clustering and allows detection of patterns in the data. In this study, PCA was done
468 using software deepTools[53].
469
470 **Data availability.**
471 Raw RNA-seq, ATAC-seq, ChIP-seq data of uncultured FL-HSPC from published reference is available in
472 Gene Expression Omnibus (GEO) with the accession code GSE111484[30].
473
474 **Acknowledgements:** We thank the technical support from the UCLA Center for AIDS research (CFAR)
475 research cores including the CFAR Gene and Cellular Therapy Core and the CFAR Humanized Mouse Core.
476 We would like also to thank Anna Sahakyan and Ruth Cortado for their help with making lentiviral vectors,
477 transducing human CD34+ HSPC, and performing humanized mouse experiments. **Funding:** This work was
478 supported by grants from the NIH (5U19AI117941, AI110297, AI145038, HL125030, HL126544), CIRM
479 (DR1-01431, TRX-01431-1), the James B. Pendleton Charitable Trust, and the McCarthy Family Foundation
480 (I.S.Y.C).

481 **Competing interests:** Dr. Irvin S.Y. Chen has a financial interest in CSL Behring and Calimmune Inc. No
482 funding was provided by these companies to support this work; Dr. Dong Sung An has a financial interest in
483 Calimmune Inc and CSL Behring that the University of California Regents have licensed intellectual
484 property invented by Dong Sung An, that is being used in the research, to Calimmune Inc. No funding was
485 provided by these companies to support this work. All other authors declare no competing interests.
486

487 Reference:

488 1 Shultz, L. D., Ishikawa, F. & Greiner, D. L. Humanized mice in translational biomedical research. *Nat*
489 *Rev Immunol* **7**, 118-130, doi:10.1038/nri2017 (2007).
490 2 Melkus, M. W. *et al.* Humanized mice mount specific adaptive and innate immune responses to EBV
491 and TSST-1. *Nat Med* **12**, 1316-1322, doi:10.1038/nm1431 (2006).
492 3 Khamaikawin, W. *et al.* Modeling Anti-HIV-1 HSPC-Based Gene Therapy in Humanized Mice
493 Previously Infected with HIV-1. *Mol Ther Methods Clin Dev* **9**, 23-32,
494 doi:10.1016/j.omtm.2017.11.008 (2018).
495 4 Biasco, L. *et al.* In Vivo Tracking of Human Hematopoiesis Reveals Patterns of Clonal Dynamics
496 during Early and Steady-State Reconstitution Phases. *Cell Stem Cell* **19**, 107-119,
497 doi:10.1016/j.stem.2016.04.016 (2016).
498 5 Kim, S. *et al.* Dynamics of HSPC repopulation in nonhuman primates revealed by a decade-long clonal-
499 tracking study. *Cell Stem Cell* **14**, 473-485, doi:10.1016/j.stem.2013.12.012 (2014).
500 6 Verovskaya, E. *et al.* Heterogeneity of young and aged murine hematopoietic stem cells revealed by
501 quantitative clonal analysis using cellular barcoding. *Blood* **122**, 523-532, doi:10.1182/blood-2013-01-
502 481135 (2013).
503 7 Brewer, C., Chu, E., Chin, M. & Lu, R. Transplantation Dose Alters the Differentiation Program of
504 Hematopoietic Stem Cells. *Cell Rep* **15**, 1848-1857, doi:10.1016/j.celrep.2016.04.061 (2016).
505 8 Suryawanshi, G. W. *et al.* The clonal repopulation of HSPC gene modified with anti–HIV-1 RNAi is
506 not affected by preexisting HIV-1 infection. *Science Advances* **6**, eaay9206,
507 doi:10.1126/sciadv.aay9206 (2020).
508 9 Esteban, J. A., Salas, M. & Blanco, L. Fidelity of phi 29 DNA polymerase. Comparison between
509 protein-primed initiation and DNA polymerization. *J Biol Chem* **268**, 2719-2726 (1993).
510 10 Paez, J. G. *et al.* Genome coverage and sequence fidelity of phi29 polymerase-based multiple strand
511 displacement whole genome amplification. *Nucleic Acids Res* **32**, e71, doi:10.1093/nar/gnh069 (2004).
512 11 He, F., Zhou, W., Cai, R., Yan, T. & Xu, X. Systematic assessment of the performance of whole-
513 genome amplification for SNP/CNV detection and beta-thalassemia genotyping. *J Hum Genet* **63**, 407-
514 416, doi:10.1038/s10038-018-0411-5 (2018).
515 12 Bleier, S. *et al.* Multiple displacement amplification enables large-scale clonal analysis following
516 retroviral gene therapy. *J Virol* **82**, 2448-2455, doi:10.1128/JVI.00584-07 (2008).
517 13 Einkauf, K. B. *et al.* Intact HIV-1 proviruses accumulate at distinct chromosomal positions during
518 prolonged antiretroviral therapy. *J Clin Invest* **129**, 988-998, doi:10.1172/Jci124291 (2019).
519 14 Patro, S. C. *et al.* Combined HIV-1 sequence and integration site analysis informs viral dynamics and
520 allows reconstruction of replicating viral ancestors. *P Natl Acad Sci USA* **116**, 25891-25899,
521 doi:10.1073/pnas.1910334116 (2019).
522 15 Modlich, U. *et al.* Insertional Transformation of Hematopoietic Cells by Self-inactivating Lentiviral
523 and Gammaretroviral Vectors. *Molecular Therapy* **17**, 1919-1928, doi:10.1038/mt.2009.179 (2009).
524 16 Montini, E. *et al.* The genotoxic potential of retroviral vectors is strongly modulated by vector design
525 and integration site selection in a mouse model of HSC gene therapy. *J Clin Invest* **119**, 964-975,
526 doi:10.1172/Jci37630 (2009).

527 17 Schroder, A. R. *et al.* HIV-1 integration in the human genome favors active genes and local hotspots.
528 *Cell* **110**, 521-529, doi:10.1016/s0092-8674(02)00864-4 (2002).
529 18 Mitchell, R. S. *et al.* Retroviral DNA integration: ASLV, HIV, and MLV show distinct target site
530 preferences. *PLoS Biol* **2**, E234, doi:10.1371/journal.pbio.0020234 (2004).
531 19 Wang, G. P., Ciuffi, A., Leipzig, J., Berry, C. C. & Bushman, F. D. HIV integration site selection:
532 analysis by massively parallel pyrosequencing reveals association with epigenetic modifications.
533 *Genome Res* **17**, 1186-1194, doi:10.1101/gr.6286907 (2007).
534 20 Lewinski, M. K. *et al.* Retroviral DNA integration: viral and cellular determinants of target-site
535 selection. *PLoS Pathog* **2**, e60, doi:10.1371/journal.ppat.0020060 (2006).
536 21 Lelek, M. *et al.* Chromatin organization at the nuclear pore favours HIV replication. *Nat Commun* **6**,
537 doi:ARTN 648310.1038/ncomms7483 (2015).
538 22 Marini, B. *et al.* Nuclear architecture dictates HIV-1 integration site selection. *Nature* **521**, 227-231,
539 doi:10.1038/nature14226 (2015).
540 23 Cattoglio, C. *et al.* Hot spots of retroviral integration in human CD34+ hematopoietic cells. *Blood* **110**,
541 1770-1778, doi:10.1182/blood-2007-01-068759 (2007).
542 24 Wu, C. *et al.* Clonal tracking of rhesus macaque hematopoiesis highlights a distinct lineage origin for
543 natural killer cells. *Cell Stem Cell* **14**, 486-499, doi:10.1016/j.stem.2014.01.020 (2014).
544 25 Aiuti, A. *et al.* Lentiviral hematopoietic stem cell gene therapy in patients with Wiskott-Aldrich
545 syndrome. *Science* **341**, 1233151, doi:10.1126/science.1233151 (2013).
546 26 Rényi, A. On measures of entropy and information. *Proceedings of the Fourth Berkeley Symposium on*
547 *Mathematical Statistics and Probability, Volume 1: Contributions to the Theory of Statistics* (1961).
548 27 Shannon, C. E. A Mathematical Theory of Communication. *Bell Syst Tech J* **27**, 379-423, doi:DOI
549 10.1002/j.1538-7305.1948.tb01338.x (1948).
550 28 Simpson, E. H. Measurement of Diversity. *Nature* **163**, 688-688, doi:DOI 10.1038/163688a0 (1949).
551 29 Wu, C. *et al.* Geographic clonal tracking in macaques provides insights into HSPC migration and
552 differentiation. *J Exp Med* **215**, 217-232, doi:10.1084/jem.20171341 (2018).
553 30 Calvanese, V. *et al.* MLLT3 governs human haematopoietic stem-cell self-renewal and engraftment.
554 *Nature* **576**, 281-286, doi:10.1038/s41586-019-1790-2 (2019).
555 31 Lu, R., Czechowicz, A., Seita, J., Jiang, D. & Weissman, I. L. Clonal-level lineage commitment
556 pathways of hematopoietic stem cells in vivo. *Proc Natl Acad Sci U S A* **116**, 1447-1456,
557 doi:10.1073/pnas.1801480116 (2019).
558 32 Rodriguez-Fraticelli, A. E. *et al.* Single-cell lineage tracing unveils a role for TCF15 in haematopoiesis.
559 *Nature* **583**, 585-589, doi:10.1038/s41586-020-2503-6 (2020).
560 33 Belderbos, M. E. *et al.* Donor-to-Donor Heterogeneity in the Clonal Dynamics of Transplanted
561 HumanCord Blood Stem Cellsin Murine Xenografts. *Biol Blood Marrow Transplant* **26**, 16-25,
562 doi:10.1016/j.bbmt.2019.08.026 (2020).
563 34 Ferrari, S. *et al.* Efficient gene editing of human long-term hematopoietic stem cells validated by clonal
564 tracking. *Nat Biotechnol*, doi:10.1038/s41587-020-0551-y (2020).
565 35 Llano, M. *et al.* An essential role for LEDGF/p75 in HIV integration. *Science* **314**, 461-464,
566 doi:10.1126/science.1132319 (2006).
567 36 Ciuffi, A. *et al.* A role for LEDGF/p75 in targeting HIV DNA integration. *Nat Med* **11**, 1287-1289,
568 doi:10.1038/nm1329 (2005).
569 37 Vanegas, M. *et al.* Identification of the LEDGF/p75 HIV-1 integrase-interaction domain and NLS
570 reveals NLS-independent chromatin tethering. *J Cell Sci* **118**, 1733-1743, doi:10.1242/jcs.02299
571 (2005).
572 38 Cherepanov, P. *et al.* Solution structure of the HIV-1 integrase-binding domain in LEDGF/p75. *Nat*
573 *Struct Mol Biol* **12**, 526-532, doi:10.1038/nsmb937 (2005).
574 39 Llano, M., Delgado, S., Vanegas, M. & Poeschla, E. M. Lens epithelium-derived growth factor/p75
575 prevents proteasomal degradation of HIV-1 integrase. *J Biol Chem* **279**, 55570-55577,
576 doi:10.1074/jbc.M408508200 (2004).

40 Eidahl, J. O. *et al.* Structural basis for high-affinity binding of LEDGF PWWP to mononucleosomes. *Nucleic Acids Res* **41**, 3924-3936, doi:10.1093/nar/gkt074 (2013).
41 Pradeepa, M. M., Sutherland, H. G., Ule, J., Grimes, G. R. & Bickmore, W. A. Psip1/Ledgf p52 binds methylated histone H3K36 and splicing factors and contributes to the regulation of alternative splicing. *PLoS Genet* **8**, e1002717, doi:10.1371/journal.pgen.1002717 (2012).
42 Huff, J. T., Plocik, A. M., Guthrie, C. & Yamamoto, K. R. Reciprocal intronic and exonic histone modification regions in humans. *Nat Struct Mol Biol* **17**, 1495-1499, doi:10.1038/nsmb.1924 (2010).
43 Hon, G., Wang, W. & Ren, B. Discovery and annotation of functional chromatin signatures in the human genome. *PLoS Comput Biol* **5**, e1000566, doi:10.1371/journal.pcbi.1000566 (2009).
44 Luco, R. F. *et al.* Regulation of alternative splicing by histone modifications. *Science* **327**, 996-1000, doi:10.1126/science.1184208 (2010).
45 Schiroli, G. *et al.* Precise Gene Editing Preserves Hematopoietic Stem Cell Function following Transient p53-Mediated DNA Damage Response. *Cell Stem Cell* **24**, 551-565 e558, doi:10.1016/j.stem.2019.02.019 (2019).
46 Shimizu, S. *et al.* A highly efficient short hairpin RNA potently down-regulates CCR5 expression in systemic lymphoid organs in the hu-BLT mouse model. *Blood* **115**, 1534-1544, doi:10.1182/blood-2009-04-215855 (2010).
47 Kim, S. *et al.* High-throughput, sensitive quantification of repopulating hematopoietic stem cell clones. *J Virol* **84**, 11771-11780, doi:10.1128/JVI.01355-10 (2010).
48 Suryawanshi, G. W. *et al.* Bidirectional Retroviral Integration Site PCR Methodology and Quantitative Data Analysis Workflow. *J Vis Exp*, doi:10.3791/55812 (2017).
49 Zhao, M., Lee, W. P., Garrison, E. P. & Marth, G. T. SSW library: an SIMD Smith-Waterman C/C++ library for use in genomic applications. *PLoS One* **8**, e82138, doi:10.1371/journal.pone.0082138 (2013).
50 Dobin, A. *et al.* STAR: ultrafast universal RNA-seq aligner. *Bioinformatics* **29**, 15-21, doi:10.1093/bioinformatics/bts635 (2013).
51 Trapnell, C. *et al.* Differential gene and transcript expression analysis of RNA-seq experiments with TopHat and Cufflinks. *Nat Protoc* **7**, 562-578, doi:10.1038/nprot.2012.016 (2012).
52 Amemiya, H. M., Kundaje, A. & Boyle, A. P. The ENCODE Blacklist: Identification of Problematic Regions of the Genome. *Sci Rep* **9**, 9354, doi:10.1038/s41598-019-45839-z (2019).
53 Ramirez, F. *et al.* deepTools2: a next generation web server for deep-sequencing data analysis. *Nucleic Acids Res* **44**, W160-165, doi:10.1093/nar/gkw257 (2016).

621 **Figures-**

622 Figure 1

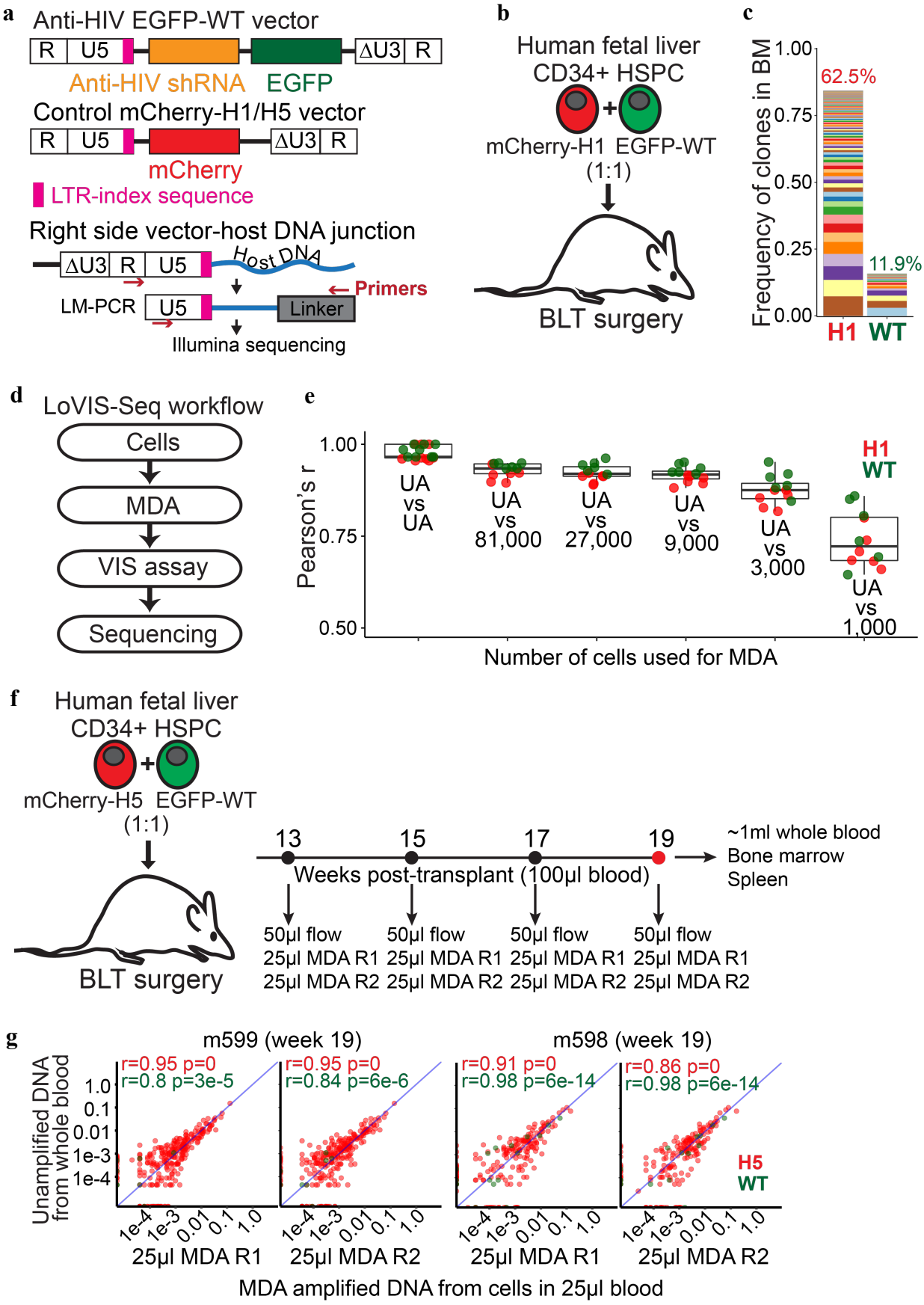

623

624 **Figure 1: LoVIS-Seq reproduces clonal distribution of entire mouse blood using 25µl blood: a**)
625 Diagram showing Anti-HIV-EGFP-WT and control mCherry-H1/H5 vectors having WT, H1, or H5 LTR-
626 index and strategy for VIS assay with LTRi-seq. **b**) Hu-BLT mouse model: Fetal liver CD34+ cells were
627 separately transduced with either anti-HIV or control vectors and transduced cells were mixed 1:1 for
628 transplant. The mix of transduced cells was transplanted in myeloablated NSG mice with a fetal thymus
629 tissue implant. **c**) Stacked bar plot showing clonal frequencies of VIS in BM of hu-BLT mouse. Clones from
630 mCherry-H1 and EGFP-WT cells were identified by corresponding LTR barcodes. In the stacked bar plot,
631 each band represents a unique VIS (HSPC clone) and thickness of the band shows clonal frequency or
632 abundance of that HSPC clone. Percentage of mCherry+ or EGFP+ cells within human cell (hCD45+)
633 population are shown on top of the corresponding stacked-bar. **d**) LoVIS-Seq workflow. **e**) Plot showing
634 Pearson's r for correlations of mCherry-H1 (red dots) and EGFP-WT (green dots) VIS clonal profiles
635 between unamplified DNA replicates and replicates of MDA-amplified DNA samples for different cell
636 numbers. **f**) Experimental protocol for longitudinal clonal tracking in humanized BLT mice. **g**) Scatter plot
637 showing VIS clonal frequencies between unamplified whole blood DNA and two replicates of MDA-
638 amplified DNA from 25µl blood at week 19 (r= Pearson's r, diagonal line is r=1) for m599 and m598. Clonal
639 frequency of mCherry-H5 (red dots) and EGFP-WT (green dots) VIS clones in unamplified DNA samples
640 (y-axis) and MDA replicates (x-axis).
641
642
643

Figure 2

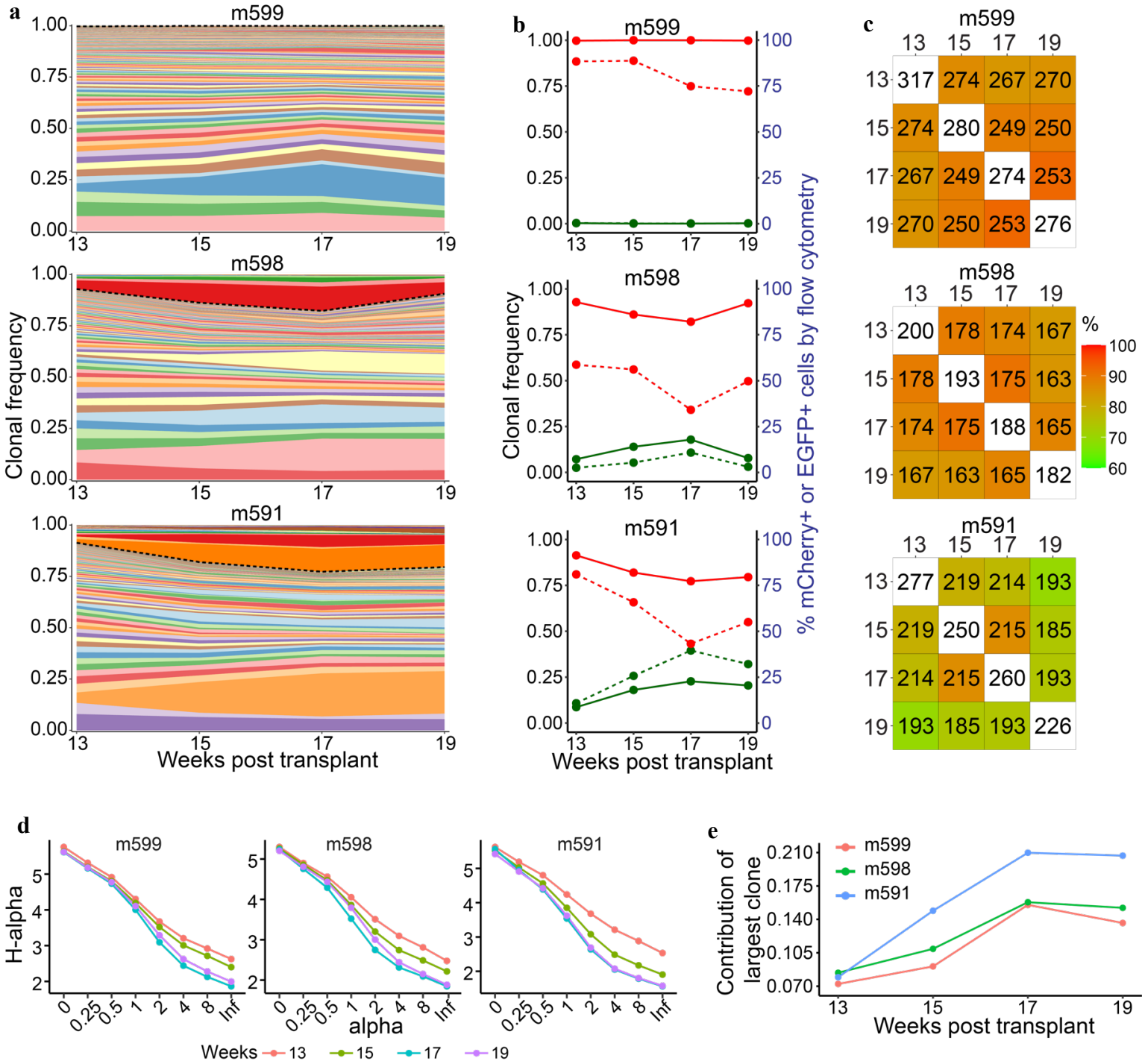

Figure 2: Longitudinal clonal tracking in hu-BLT mice: a) Area plots show clonal repopulation in whole blood over time from week 13-19. Each colored band is a unique VIS clone and thickness of the band corresponds to frequency of the VIS clone. Dashed black line separates mCherry-H5 VIS clones (below) and EGFP-WT VIS clones (above). **b**) Line plots show changes over time in the total frequency of mCherry-H1 VIS clones (solid red line) and total frequency of EGFP-WT VIS clones (solid green line) as well as percentages of mCherry+ cells (dashed red line) and EGFP+ cells (dashed green line). **c**) Heatmaps showing

652 percentage change in shared clones between two timepoints. Digits inside white tiles on the diagonal show
653 number of VIS detected at each time point. Colors of each heatmap tile correspond to percentage of clones
654 shared and color key is provided on the right. Digits in each tile show the number of VIS shared between two
655 timepoints. **d**) Renyi's diversity profiles evaluated using raw count data from two replicates at each
656 timepoint and by varying value of alpha. Renyi's diversity profiles are arranged with highest diversity at the
657 top to lowest at the bottom. Topmost curve with no overlap or intersection with any other curve has the
658 highest overall diversity. Diversity of curves that overlap or intersect is undefined. **e**) Line plot showing
659 contribution of highest contributing clone at different timepoints. Values reported are exp(H(alpha)) at
660 alpha=∞.
661
662
663
664
665
666
667
668
669
670
671
672
673
674
675
676
677
678
679
680
681
682
683
684
685

686 Figure 3

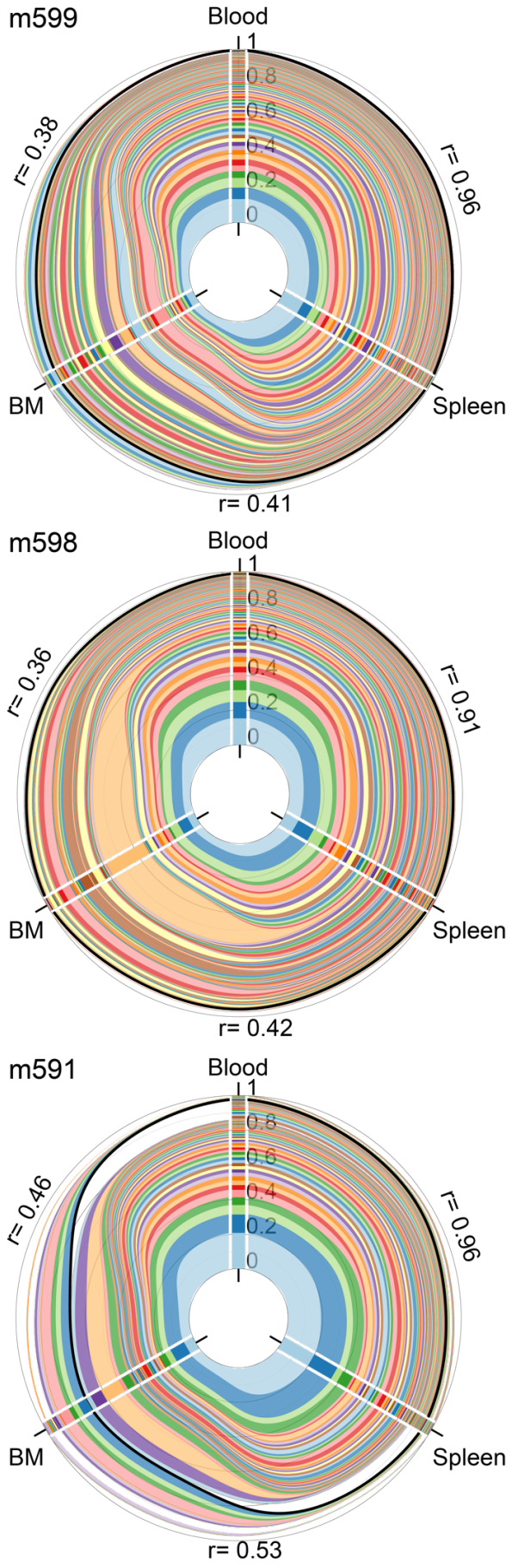

687

Figure 3: Unique clonal sharing pattern between different tissues: Polar area plots of clonal expansion and sharing in peripheral blood, spleen, and bone marrow (BM). There are three axes, one for each tissue. Stacked bar plot on each axis shows size distribution of clones in the tissue. Each colored stack represents a VIS clone and its thickness shows abundance of the clone. Clones shared between tissues are connected using ribbons with colors matching the clone's stack color in the bar plot. Black line encompasses total size distribution of persistent clones. Pearson's r values are shown in black.

722 Figure 4

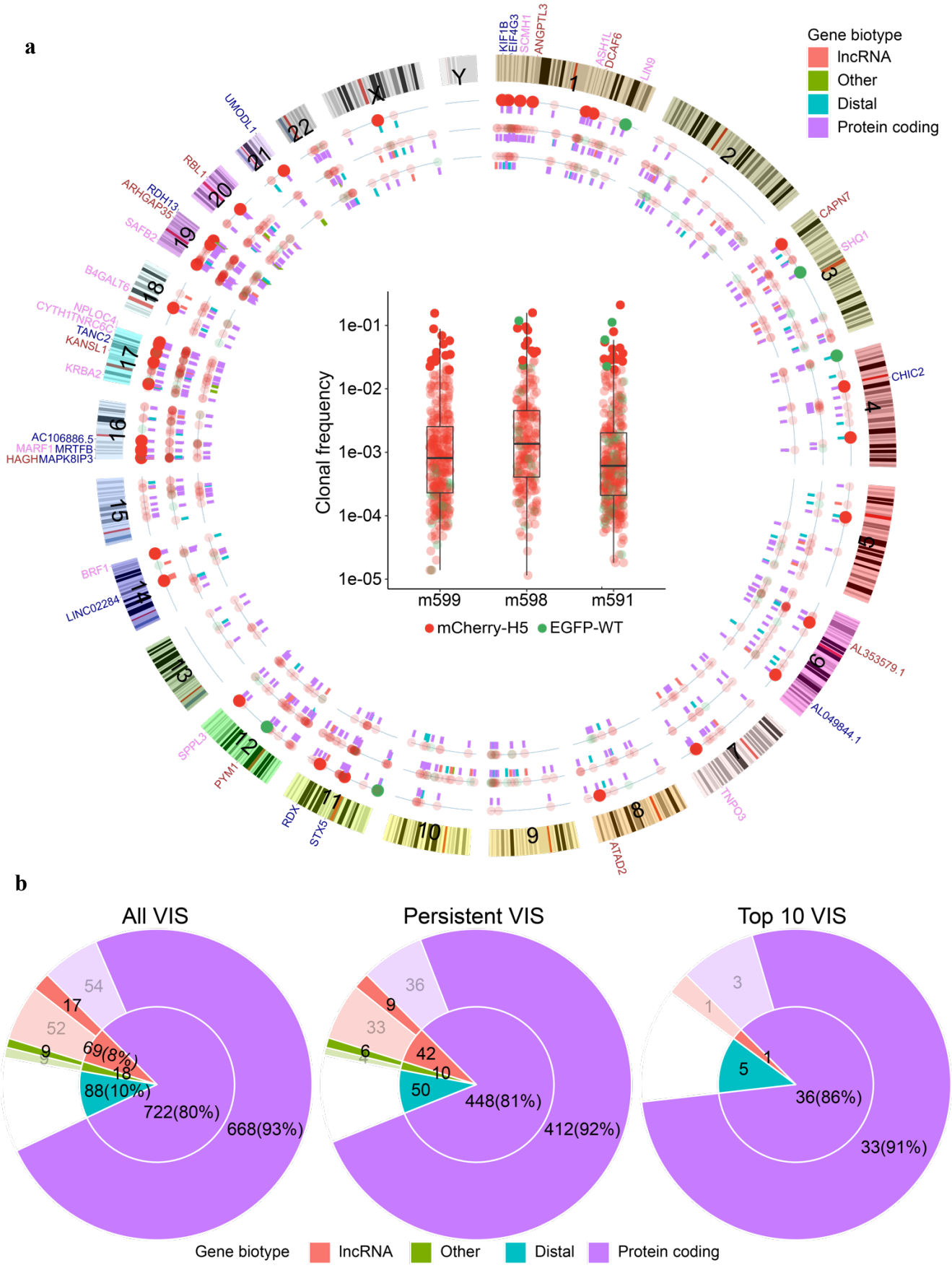

723

724 **Figure 4: Chromosomal distribution of VIS and its bias for transcriptionally active genes: a**) Circos
725 plot shows genomic location of all 792 mCherry-H5 (red dots) and 105 EGFP-WT (green dots) VIS from
726 mice m599, m598, and m591. Box plots in the center show maximum frequency of mCherry-H5 (red dots)
727 and EGFP-WT (green dots) VIS clones in mice m599, m598, and m591 over 6 weeks. Genomic location of
728 mCherry-H5 (red dots) and EGFP-WT (green dots) VIS clones are plotted on three concentric circles
729 depending on their maximum frequency over 6 weeks: Low frequency clones with maximum frequency
730 below the 1st quartile value (innermost circle), High frequency clones above 3rd quartile value (outermost
731 circle), and Medium frequency clones between 1st and 3rd quartile (middle circle). Top 10 high frequency
732 VIS clones are shown in darker colors. Functional classification of VIS-proximal genes is shown by short
733 line segments, color coded as in the legend. Gene symbols above ideograms represent genes proximal to the
734 top 10 VIS clones from mice m599 (blue), m598 (brown), and m591 (light pink). **b**) Classification of all,
735 persistent, and Top 10 VIS clones based on biotype of proximal gene. Inner pie chart shows clones classified
736 based on gene biotype of the most proximal gene. Outer Donut plots show number of VIS and numbers in
737 bracket show % of VIS proximal to active (dark color) or inactive (faded colors) genes. Active proximal
738 genes have FPKM >1.
739

Figure 5

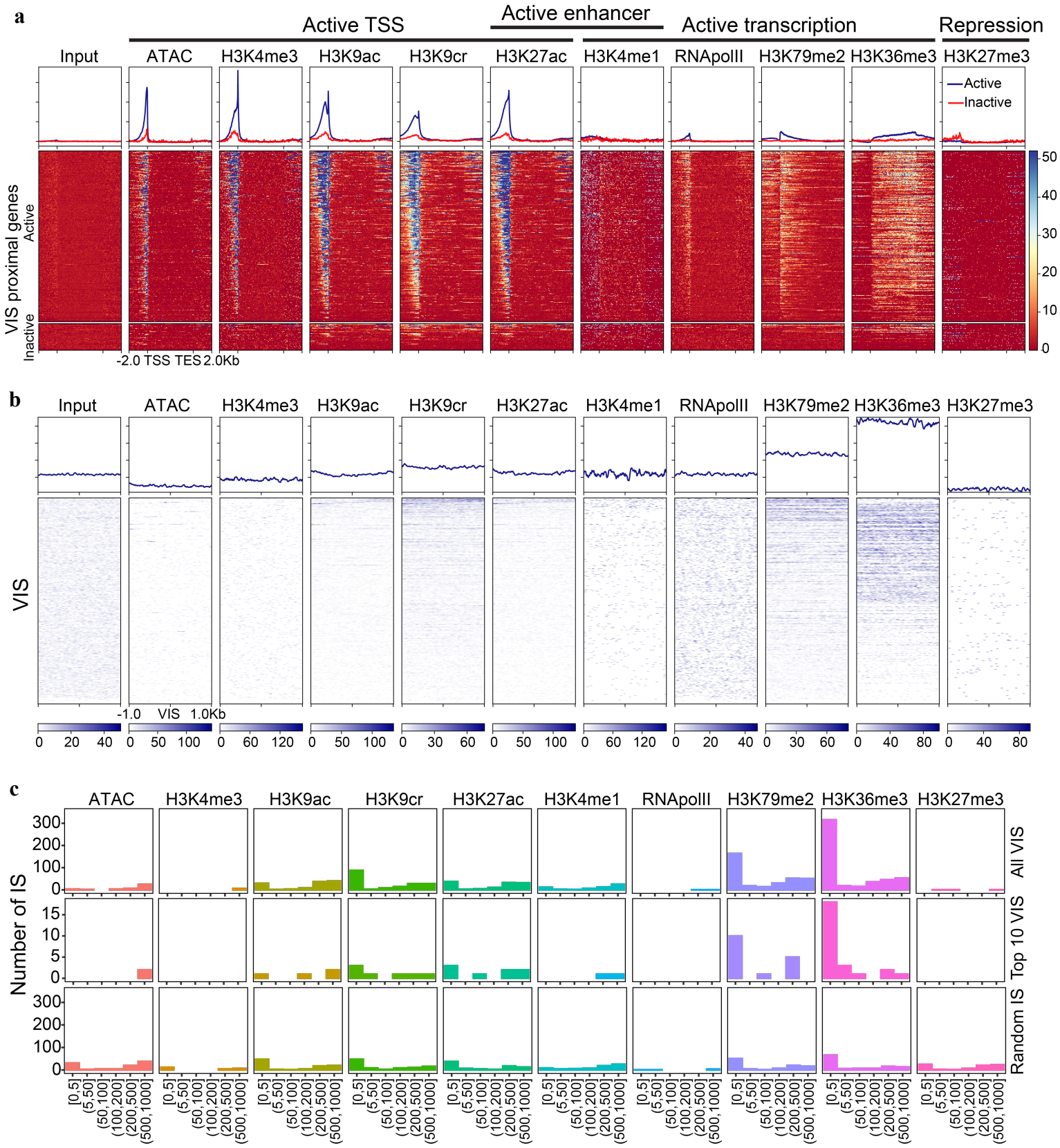

Figure 5: Epigenetic determinants of vector integration: a) Profile plots and heatmap for 10 chromatin features and input sample in active and inactive VIS-proximal genes in uncultured FL-HSPC. Profile plots

744 show mean score for active (blue line) and inactive (red line) proximal genes. Score is calculated from
745 normalized read count (RPKM) for each sample. Each row in heatmap shows expression level of 10
746 chromatin features in proximal genes from TSS to TES with 2Kb flanks upstream and downstream. Color
747 scale key shows range of normalized expression. **b**) Profile plots and heatmaps for 10 chromatin features in
748 region flanking ±1Kb of each VIS. Profile plots showing mean scores over ±1Kb region flanking VIS. Each
749 row in the heatmap shows the expression level of 10 chromatin features in regions flanking ±1Kb of VIS.
750 Individual color scale key shows the range of normalized expression for corresponding features. **c**) Bar plots
751 show number of VIS within ±1Kb of enriched region (peak) of different chromatin features. VIS clones and
752 random IS are binned by absolute distance in base pairs (bp) between the enriched region and IS. Bars show
753 number of VIS in each bin. Top panel shows binning for all VIS, middle panel shows top 10 VIS clones, and
754 bottom panel shows random IS falling within ±1Kb of enriched region.
755